



Numerical Study of Bed Topography Variations Owing to Placement of Triad Series of Vertical Bridge Piers Installed in a 180-degree Bend with Different Relative Radii Using SSIIM Numerical Model

Mohammad Vaghefi¹ · Sahar Moradi¹ · Chonoor Abdi Chooplou¹

Received: 7 July 2019 / Accepted: 4 December 2020 / Published online: 18 January 2021
© Shiraz University 2021

Abstract

In this paper, the scouring around a triad series of vertical bridge piers located in a bend is investigated using SSIIM software. To this end, some of the most essential parameters such as the relative radius and the bridge pier position in both transverse and longitudinal directions to the flow have been examined. Then the bed topography variations have been detected within a flume. It is worth mentioning that the experiments have been conducted in a 180-degree sharp bend in the presence of the bridge piers. The available experimental results were used to ensure correctness of the simulated output data. Accordingly, it is evident that the simulated model not only is capable of estimating the amount of the maximum scour and sedimentation but also can effectively predict their position using an experimental model. Based on the results, it is indicated that the maximum scour depth is reported in the case of the bridge pier transverse to the flow installed at the 60-degree position of the bend with a relative radius of 5. Under these circumstances, the maximum depth of scour is evaluated to be 1.14 times the depth of flow at the beginning of the bend. Also, the maximum volume of scour around bridge piers has been detected in this case.

Keywords Scouring · Bed topography variations · Relative radius · 180° sharp bend · SSIIM model

List of Symbols

SSIIM	The numerical model for calculating water and sedimentation in channel	k	The turbulent flow kinetic energy
CFD	Computational fluid dynamics	P	Total pressure
R	The central curvature radius of the bend	a	The reference area equivalent to roughness height
B	The channel width	D_{50}	The average sediment diameter
R/B	The relative curvature radius	g	Acceleration of gravity
Q	The flow discharge	ρ_s	Sediment density
D	The pier diameter	ρ_w	Water density
d	The distance between the piers	τ	Bed shear stress
Y	The upstream flow depth	τ_C	Critical bed shear stress
Z	The bed topography variations	δ_{ij}	Kronecker delta
θ	The angles from the beginning of the bend	ε	The turbulent flow kinetic energy loss
U	The velocity component	ν	Water kinematic viscosity
		ν_T	Vortex viscosity
		C_{bed}	Near bed suspended particles concentration
		q_b	Bed load
		$d_{s_1 max}$	The maximum scour depth around piers
		$d_{s_2 max}$	The maximum scour depth of the second scour hole
		h_{max}	The maximum sedimentation height
		L	The length of the rectangle surrounding the main scour hole
		W	The width of the rectangle surrounding the main scour hole

✉ Mohammad Vaghefi
Vaghefi@pgu.ac.ir

Sahar Moradi
saharmorady1386@gmail.com

Chonoor Abdi Chooplou
chonoorabdi@yahoo.com

¹ Department of Civil Engineering, Persian Gulf University, Bushehr 7516913817, Iran

- A The main scour hole area
V The main scour hole volume

1 Introduction

Rivers are constantly changing in terms of size, shape, path and pattern, and respond to natural forces that change along their continuum. Parameters such as the flow discharge, the sediment discharge, the grade of bed sediment and the sediments deposited on riverbanks cause the mentioned changes, classifying the rivers into groups. Regarding the planform of the rivers, they are subdivided into straight and meandering. In the planform of meandering rivers, a series of regular sinuous curves, bends, loops and turns directly connected to each other in the channel of a river are visible. The flow pattern in the meandering river seems to be rather complicated, and the river bend has been of interest to hydraulic engineers due to the special spiral flow regime. Rivers as a natural flow of running water generally flow in an irregular pattern instead of following the straight path. Therefore, investigating morphology of rivers has been of great importance. The primary characteristic of the flow in an open-channel bend is the strong secondary flow known as the secondary motion, the secondary circulation, the latitudinal flow and the latitudinal circulation.

Bridges are a critical component of a nation's infrastructure to provide continuous access for a road network. Every year, many bridges fail worldwide mainly due to scouring at their piers (Johnson and Dock 1998). The flow pattern around piers is naturally complicated and becomes more complicated when a scour hole forms. The hole expansion around piers causes the removal of sediments, and the bridge may then collapse. Hence, the scour mechanism needs to be analyzed.

As already mentioned, the flow pattern in the bend as well as the complexity of flow around the cylindrical pier makes the flow pattern more complicated. As bridges are mainly placed in a bend of the river, and considering the different flow structures in the bend and as well as the importance of flow structure and scour depth evaluation around the piers, more detailed analysis of flow structure around the piers is needed. The following is a brief introduction to some of the research efforts from the literature. Graf and Istiarto (2002) investigated the flow pattern around a cylinder on a moving bed by using an acoustic Doppler velocity profiler (ADVP) and reported the resultant vortices. Bozkus and Yildiz (2004) analyzed the scour around a bridge with a single circular pier in a straight channel and found that the local scour depth decreased considerably as the inclination angle of the pier toward downstream was increased. Elsebaie (2013) worked on the scour around a cylindrical pier and reported the maximum scour depth at the upstream

side of the pier, directly proportional to time and the flow rate. Fael et al. (2016) studied the influence of the shape and angle of the pier on scour depth around a single pier in a straight path. In fact, 5 types of piers were used through the experiments. They realized that the value of the pier shape coefficient may be assumed 1 for rectangular piers with round corners and 1.2 for the cases with sharp corners. Ben Mohammad Khajeh et al. (2017) evaluated the depth and the location of scour around an inclined cylindrical bridge pier in the apex of a sharp 180-degree bend. The outcomes indicated that the maximum and the minimum scour depths happened around the pier inclined toward the outer bank and the inner bank, respectively. Surprisingly, by placing the pier with its inclination toward the outer bank, alternating sedimentary dunes appeared at the downstream side of the pier in an area adjacent to the inner bank. Vaghefi et al. (2020) analyzed the scouring affected by the presence of a rigid T-shaped spur dike around bridges with a 90° pier in a 180° channel with a sharp bend. The findings suggested that the installation of the T-shaped spur dike on the outer bank remarkably reduced the scour around the bridge pier. Moreover, installation of a spur dike at the 70° position on the outer bank resulted in the greatest influence, reducing the scour by 45 percent compared to the case with no spur dikes installed. Ben Mohammad Khajeh and Vaghefi (2020) studied the effects of abutments in the presence of a pier on scour depth in a sharp 180-degree bend. They found that the maximum scour depth was detected at the upstream side of the outer abutment in all tests.

The numerical model compared to the laboratory experiments appears to be less time- and cost-consuming in terms of the determination of the impact of some parameters on scour. Investigation of parameters such as the radius of curvature in a laboratory requires large space and is time- and cost-consuming, whereas, for researchers, the numerical model is a low-cost and easy-to-use way to achieve the desired results. Several studies have been carried out on this matter and some studies are mentioned below. Olsen and Melaen (1993) developed a 3D simulation model to model the flow pattern around a bridge for the determination of the water level variations and the bed scour around the bridge piers. Richardson and Panchang (1998) analyzed the flow pattern around a cylindrical pier by using FLOW-3D software and examined the impact of local scour on the flow pattern. Tseng et al. (2000) represented a 3D numerical model by which the flow pattern around a cylindrical pier exposed to a steady flow was modeled using the finite volume method by solving no compressible fluid equations. Yen et al. (2001) could model bed elevation changes and flow pattern around cylindrical bridge piers by combining a 3D flow model with a scour model. In fact, large eddy simulation (LES) model was applied in order to model the turbulence and the bed shear stress. Roulund et al. (2002) modeled the flow

around a bridge pier using 3D numerical model. The effect of roughness thickness of the boundary layer, the bed coarseness and inclination of pier with respect to the transverse direction on horseshoe vortices formation has been studied. The results indicate that an increase in horseshoe vortices length is intimately associated with increasing the Reynolds number. Salahedin et al. (2004) applied Fluent software for simulating the divergent flow pattern around the pier under clear water condition. Elsaeed (2011) investigated the scour pattern around the bridge piers using SSIIM and achieved acceptable conclusions. In this paper, scour evaluation by SSIIM was regarded more feasible than other methods because the computational cost and time have significantly decreased. Akib et al. (2014) studied the scour and its maximum depth around a real bridge pier using SSIIM2 numerical software. Mohamed et al. (2015) developed a 3D numerical model to simulate scour around bridge piers employing SSIIM software. Ehteram and Meymand (2015) modeled the flow and sediment where the bridge becomes narrower using SSIIM2 in 3D space. Bassier et al. (2015) applied SSIIM to simulate the scour around a rectangular abutment. Ghobadian and Basiri (2016) calculated the local scouring and sedimentation pattern at a laboratory 60-degree channel using 3D SSIIM software. Azizi et al. (2016) studied the flow around a bridge pier surrounded by submerged vanes using Fluent software. Wang et al. (2016) determined scour around twin circular bridge piers along a straight path. Karimi et al. (2017) carried out an experimental study on the effect of inclination angle of the bridge piers on the scouring process through a straight channel. Hamidi and Siadatmousavi (2017) applied a SSIIM numerical model in order to simulate the flow pattern and the scour pattern around the bridge piers placed in a straight path. According to their results, although SSIIM numerical model evaluated the scour depth effectively, it overestimated the scour depth between the piers. Vaghefi et al. (2017) conducted a research work on the flow pattern around a T-shaped spur dike influenced by attractive and repelling protective structures using SSIIM numerical model. Khayyun and Mouhamed (2018) analyzed the flow pattern and sediment transport along a river. Based on the findings, SSIIM model appeared to be a perfect dynamic model to assess and evaluate the sediment transport. Hämmerling et al. (2018) recorded velocity distribution and bed elevation changes of the Warta river, as a meandering river, using SSIIM. Ezzeldin (2019) compared numerical analysis with experimental results and realized that the scour depths around a spur dike are roughly similar in both models. In other words, SSIIM is able to simulate the scour and sedimentation with an acceptable accuracy. Asadollahi et al. (2019) made experimental and numerical comparisons between flow and scour pattern around single and triad series of piers located in a sharp 180-degree bend. Asadollahi et al. (2020) employed SSIIM numerical model

to examine the 3D flow and scour pattern around pier groups placed in transverse direction. The results demonstrated that changing the position of the bridge piers in the channel has an insubstantial impact on the maximum scour value, yet the amount of the maximum sedimentation increased by 12% after relocating the piers from the 60- to the 90-degree angle; however, relocating them from the 90- to the 120-degree position led to a 42% reduction in the maximum sedimentation. Rasaei et al. (2020) measured the maximum depth and volume of scour hole around piers in a 90° convergent bend, with a central curvature radius of 170 cm, of a river. The cylindrical pier with a diameter of 60 mm was prepared and installed in positions of 0°, 30°, 45°, 60° and 75° of a 90° convergent bend to consider the local scour in clear water mode. A comparison between experimental and numerical results revealed that increasing the convergence in the bend increased the continuity between flow lines as well as the intensity of the secondary currents. SSIIM-2 numerical model efficiently simulates the scour pattern in a 90-degree convergent bend, and in the numerical case, it showed a good agreement with the experimental results.

A recent review of the literature on this topic indicates that the scour pattern around piers placed in longitudinal and transverse directions to the flow in a bend, the effect of parameters such as the pier position and the changes in radius of curvature have not yet been discussed. Accordingly, this manuscript intends to provide reliable knowledge on this matter. Moreover, based on numerical studies, SSIIM program can be used efficiently for the simulation of the scouring.

2 Methodology

2.1 The Experimental Model for Verification

Vaghefi et al. (2018) performed the experiments using a flume with a 180-degree bend in the advanced laboratory at Persian Gulf University. The flume is equipped with an upstream 6.5-m-long straight reach and a downstream 5.1-m-long straight reach which are connected to each other by a 180-degree bend with an inner radius of 1.5 m and an outer radius of 2.5 m. In addition, to better strengthen the flume and protect its wall, which is made of glass, a metal frame is utilized. The flume is 70 cm deep and 1 m wide (B), and the relative radius of the bend to its width (R/B) is 2 according to Leschziner and Rodi (1979); it is qualified as a sharp bend.

The flume has a bed slope of 0.001, covered by a layer of 30-cm-thick sand with an average diameter of 1.5 mm and a deviation coefficient of 1.14. The inlet discharge is 70 l/s, which is close to the incipient motion. Cylindrical bridge piers with a 5-cm diameter and a 15-cm

center-to-center distance are placed in the middle of the flume in both transverse and longitudinal directions to the flow. A schematic view of the bridge piers is presented in Fig. 1.

2.2 The Numerical Model and Equations Governing the Flow

The main advantage of SSIIM model compared to other CFD models is its simulating ability in terms of sediment transport along a movable bed in complicated geometry. The Navier–Stokes equation for turbulent flow in a general three-dimensional geometry is solved to obtain the water velocity. The k – ϵ model is used for calculating the turbulent shear stress.

The Navier–Stokes equations, non-compressible and constant density flow can be modeled as defined by Eq. (1):

$$\frac{\partial U_i}{\partial t} + U_j \frac{\partial U_i}{\partial x_j} = \frac{1}{\rho_w} \frac{\partial}{\partial x_i} (-P\delta_{ij} - \rho \overline{u_i u_j}) \quad (1)$$

Here, x is distance, U denotes velocity in three directions, P presents total pressure, and δ_{ij} is Kronecker delta that is 1 if $i=j$; otherwise, it is 0 (Olsen 2014).

The left term on the left side of the equation is the local acceleration, and the next term is the convective acceleration.

The first term on the right-hand side is the pressure term. The second term on the right side of the equation is the Reynolds stress term. To evaluate this term, a turbulence model is required.

The equations are discretized with a control volume approach. An implicit solver is used, also for the multi-block option. The SIMPLE method is the default method used for pressure correction. The power-law scheme or the second-order upwind scheme is used in the discretization of the convective terms (Olsen 2014).

The eddy viscosity concept is introduced with the Boussinesq approximation to model the Reynolds stress term using Eq. (2)

$$-\overline{u_i u_j} = \nu_T \left(\frac{\partial U_j}{\partial x_i} + \frac{\partial U_i}{\partial x_j} \right) + \frac{2}{3} k \delta_{ij} \quad (2)$$

The first term on the right side of the equation forms the diffusive term in the Navier–Stokes equation. The second term is often neglected. The third term on the right side is incorporated in to the pressure. It is very small and usually not of any significance (Olsen 2014).

The k – ϵ model calculates the eddy viscosity by Eq. (3)

$$\nu_T = c_\mu \frac{k}{\epsilon} \quad (3)$$

K is turbulent kinetic energy modeled as Eq. (4):

$$\frac{\partial k}{\partial t} + U_j \frac{\partial k}{\partial x_j} = \frac{\partial}{\partial x_j} \left(\frac{\nu_T}{\sigma_k} \frac{\partial k}{\partial x_j} \right) + P_k - \epsilon \quad (4)$$

where P_k is given by Eq. (5):

$$P_k = \nu_T \frac{\partial U_j}{\partial x_i} \left(\frac{\partial U_j}{\partial x_i} + \frac{\partial U_i}{\partial x_j} \right) \quad (5)$$

The dissipation of k is denoted by ϵ and modeled as (Olsen 2014):

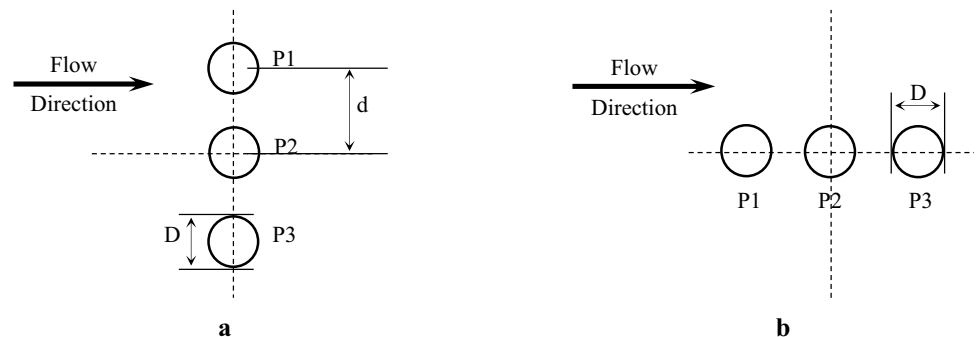
$$\frac{\partial \epsilon}{\partial t} + U_j \frac{\partial \epsilon}{\partial x_j} = \frac{\partial}{\partial x_j} \left(\frac{\nu_T}{\sigma_\epsilon} \frac{\partial \epsilon}{\partial x_j} \right) + C_{\delta 1} \frac{\epsilon}{K} P_k + C_{\delta 2} \frac{\epsilon^2}{K} \quad (6)$$

In the above-mentioned equations, for k – ϵ model, the constant values are defined as follows and these cannot be changed by the user (Olsen 2014):

$$c_\mu = 0.09 \quad C_{\epsilon 1} = 1.44 \quad C_{\epsilon 2} = 1.92 \quad \sigma_\epsilon = 1.3$$

For suspended load, Olsen (2014) developed a formula for the equilibrium sediment concentration, C_{bed} , close to bed:

Fig. 1 A schematic view of the piers placed in (a) transverse and (b) longitudinal directions to the flow



$$C_{bed} = 0.015 \frac{D_{50}^{0.3} \left[\frac{\tau - \tau_c}{\tau_c} \right]^{1.5}}{a \left[\frac{(\rho_s - \rho_w)g}{\rho_w v^2} \right]^{0.1}} \tag{7}$$

The sediment particle diameter is denoted by D_{50} , a is a reference level set equal to the roughness height, τ is the bed shear stress, τ_c is the critical bed shear stress for movement of sediment particles according to shields curve, ρ_w and ρ_s are the density of water and sediment, ν is the viscosity of water (m^2/s), and g is the acceleration of gravity (Olsen 2014).

In addition to the suspended load, bed load q_b can be calculated. Olsen’s formula for bed load is used as Eq. (8):

$$\frac{q_b}{D_{50}^{1.5} \sqrt{\frac{(\rho_s - \rho_w)g}{\rho_w}}} = 0.053 \frac{\left[\frac{\tau - \tau_c}{\tau_c} \right]^{2.1}}{D_{50}^{0.3} \left[\frac{(\rho_s - \rho_w)g}{\rho_w v^2} \right]^{0.1}} \tag{8}$$

Here, D_{50} is the particle diameter, a is a base surface equivalent to roughness height, τ is the bed shear stress, and τ_c denotes the critical shear stress for incipient motion of particles on the bed (Olsen 2014).

2.3 The Boundary Conditions and Meshing

The inlet discharge is defined, and the gradient of all parameters is also assumed to be 0. The outlet discharge has been introduced as one of the outlet boundary conditions. ϵ gradient and k value in water surface level are 0 as well as the discharge crossing bed and walls. Also, the gradient of loss of kinetic energy and the value of kinetic energy in the water surface is zero. The flux passing the bed and walls is zero.

During simulation, in order to achieve more accurate and reliable findings, in both bridge pier modes in transverse and longitudinal directions to the flow, a finer mesh consisting of 61 and 55 radial sections (latitudinal) and 53 and 69 longitudinal sections, in addition to 7 altitudinal sections,

is applied as depicted in Fig. 2. In fact, non-uniformity was visible in mesh in deeper parts so that the mesh used near the bed and the water surface was finer compared to that used in other parts.

2.4 Initial Conditions in Modeling

The flow properties during all experiments are $Q=90$ l/s, $Y=18$ cm and $Fr=0.3$. Q is discharge, Y is water depth at the bend entrance, and Fr is the Froude number in straight parts at the upstream side of the bend. The flume walls are solid, and only the bed is erodible and analyzed under clear water conditions since the maximum scour depth occurs in clear water. On the other hand, the scour holes were not filled by the sediment transported from upstream. The piers were modeled in both pier modes in transverse and longitudinal directions to the flow in different positions, installed in the 180-degree bend with relative radii of 2, 3, 4 and 5, as displayed in Table 1.

As shown in the second column of the table, a symbol is assigned to each modeling. P represents the bridge pier. and T and L denote the transverse and longitudinal directions, respectively. In naming the process of models, the first and second numbers refer to the relative radius of the bend and the bridge pier position, respectively. For instance, model 1, labeled as PT2-60, indicates that the bridge piers are installed in a transverse direction to the flow in a bend with a relative radius of 2 at the 60-degree position.

2.5 Experimental Verification of the Numerical Model

First, the numerical model has to be calibrated by an experimental model, and its ability has to be proved. To verify this model, the findings of Vaghefi et al. (2018) have been considered.

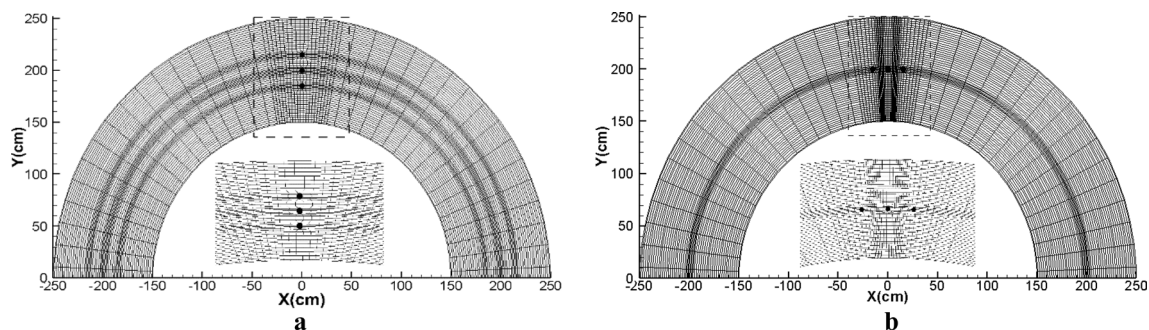


Fig. 2 Mesh used when the piers are placed in a transverse and b longitudinal directions to the flow

Table 1 Model characteristics

Number of test	Symbol of test	The pier placement in the flume	R/B	The position of bridge piers (°)
1	PT2-60	T	2	60
2	PT3-60	T	3	60
3	PT4-60	T	4	60
4	PT5-60	T	5	60
5	PL2-60	L	2	60
6	PL3-60	L	3	60
7	PL4-60	L	4	60
8	PL5-60	L	5	60
9	PT2-90	T	2	90
10	PT3-90	T	3	90
11	PT4-90	T	4	90
12	PT5-90	T	5	90
13	PL2-90	L	2	90
14	PL3-90	L	3	90
15	PL4-90	L	4	90
16	PL5-90	L	5	90
17	PT2-120	T	2	120
18	PT3-120	T	3	120
19	PT4-120	T	4	120
20	PT5-120	T	5	120
21	PL2-120	L	2	120
22	PL3-120	L	3	120
23	PL4-120	L	4	120
24	PL5-120	L	5	120

2.5.1 Verification of the Numerical Model with Bridge Piers Transverse to the Flow

Asadollahi et al. (2019) studied the verification process of SSIIM numerical model with experimental model when the bridge piers are in transverse direction with respect to the flow. Based on comparisons, the SSIIM numerical model is capable of simulating the scour pattern in the 180° sharp bend with the bridge piers. In both mentioned models, the maximum scour value and the maximum sedimentation are approximately the same.

2.5.2 Verification of the Numerical Model with Bridge Piers Longitudinal to the Flow

Figure 3 displays the bed topography in numerical model in the 180° bend with bridge piers longitudinal to the flow. Considering the figure, it is clear that the presented numerical model is in accordance with the experimental one from Vaghefi et al. (2018) in terms of occurrence place

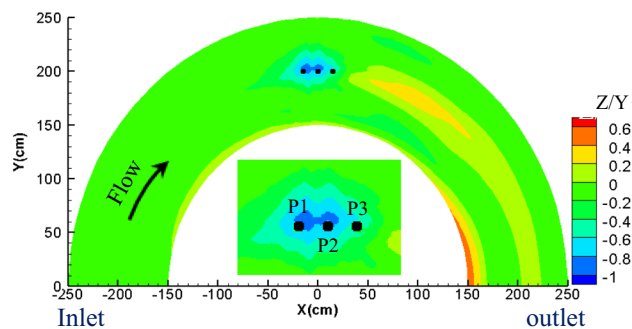


Fig. 3 Bed topography in the numerical model with bridge piers placed longitudinal to the flow

and the maximum scour. The maximum scour in the experimental model around the bridge piers is 1.04 times the flow depth at beginning of the bend and is recorded at the 89° section, while, for the numerical model, this amount decreases to 0.94 times the flow depth at the beginning of the bend at the 87° section. As evident, the dimensionless maximum amount of sediment in both models is estimated 0.6 and is deposited in the vicinity of the inner bank.

Figure 4 demonstrates a sample of the latitudinal profile of the bed for both numerical and experimental models in 4 sections at 60°, 86°, 90° and 94°. According to Fig. 4a, at the 60° section located before the bridge piers in both models, at the inner bank of the bend, sedimentation is equivalent to 1–5% of the flume width at the inner bank. As shown in Fig. 4b–d, at 86°, 90° and 94° sections, where the bridge piers are placed, SSIIM is able to simulate Vaghefi et al. (2018) experimental model accurately so that sedimentation appears at the beginning of the flume in both models and the maximum scour occurs around the piers. The maximum scour is recorded at the 86° section around the first bridge pier.

The scour pattern around the middle bridge pier, in both models, is approximately similar, whereas the maximum scour, in the experimental model, occurs around the middle bridge pier located between upstream and middle one. Also, it is evident that around the downstream bridge pier, compared to the other bridge piers, less scour occurs in both models, and the maximum scour of 0.6 and 0.8 times the incoming flow depth formed around the third bridge pier in the numerical model and experimental model from Vaghefi et al. (2018).

A point-to-point comparison between the numerical model and the experimental model from Vaghefi et al. (2018) in bridge piers longitudinal to the flow direction is provided in Fig. 5. Based on the bisector line, values in both models are intimately equal and mainly concentrated in a 20% error range.

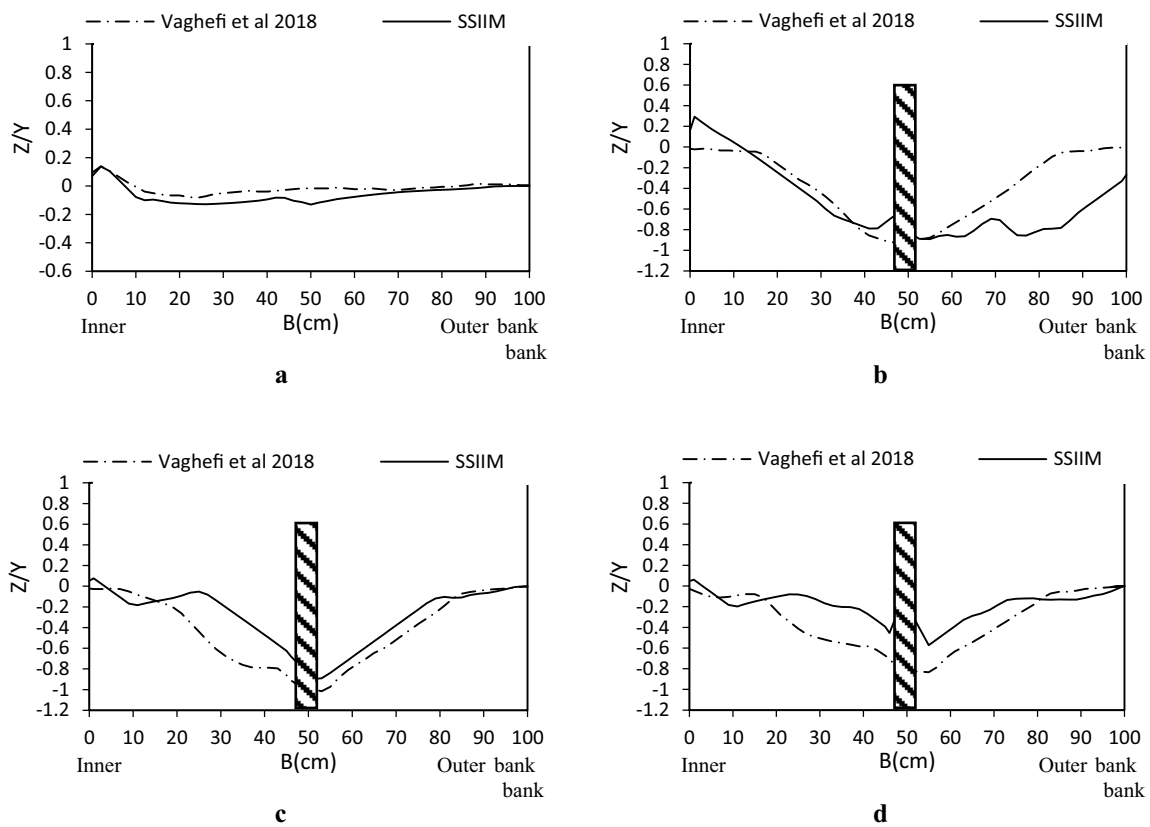


Fig. 4 A comparison between numerical and experimental latitudinal profiles of the bed in a 60-, b 86-, c 90- and d 94-degree sections

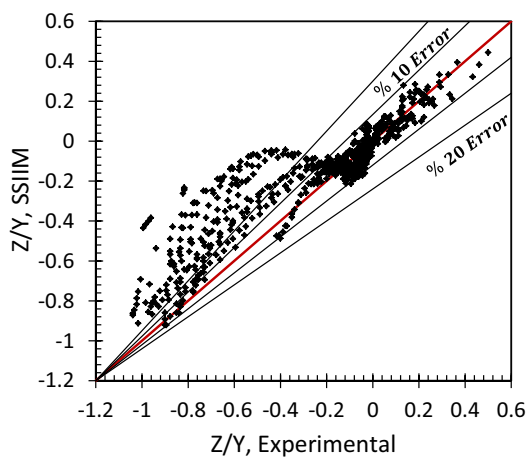


Fig. 5 A comparison between the data related to bed topography of the numerical model and the experimental model from Vaghefi et al. (2018)

3 Results

In this section, the results related to bed topography variations are discussed. In fact, the effect of pier relocation and

the changes of bend radii on bed topography in channel will be analyzed.

3.1 The Bed Topography Variations

The bed topography for models with piers placed in both transverse and longitudinal directions to the flow, which is affected by the mentioned parameters as well as the magnification of the scour hole developed around piers, is depicted in Figs. 6, 7 and 8. In fact, the presence of the piers along the bend leads to the flow pattern changes, forming vortices around the piers and resulting in variations in bed topography. In the case where the piers are situated in the middle of the bend, the scour is estimated to increase, and the excavated sediments are accumulated at the downstream side of the piers. Finally, the sedimentary stacks gradually move into the inner bank owing to the secondary flow motion in close-bed layers combined with the streamwise velocity.

A glance at Fig. 6a, in the sharp bend with a relative radius of 2, reveals that the piers are exposed to the main scour hole in addition to a secondary scour hole downstream. The secondary scour hole formation is attributed to the presence of the secondary flows together with sedimentary stacks at the inner bank. By changing the pier orientation

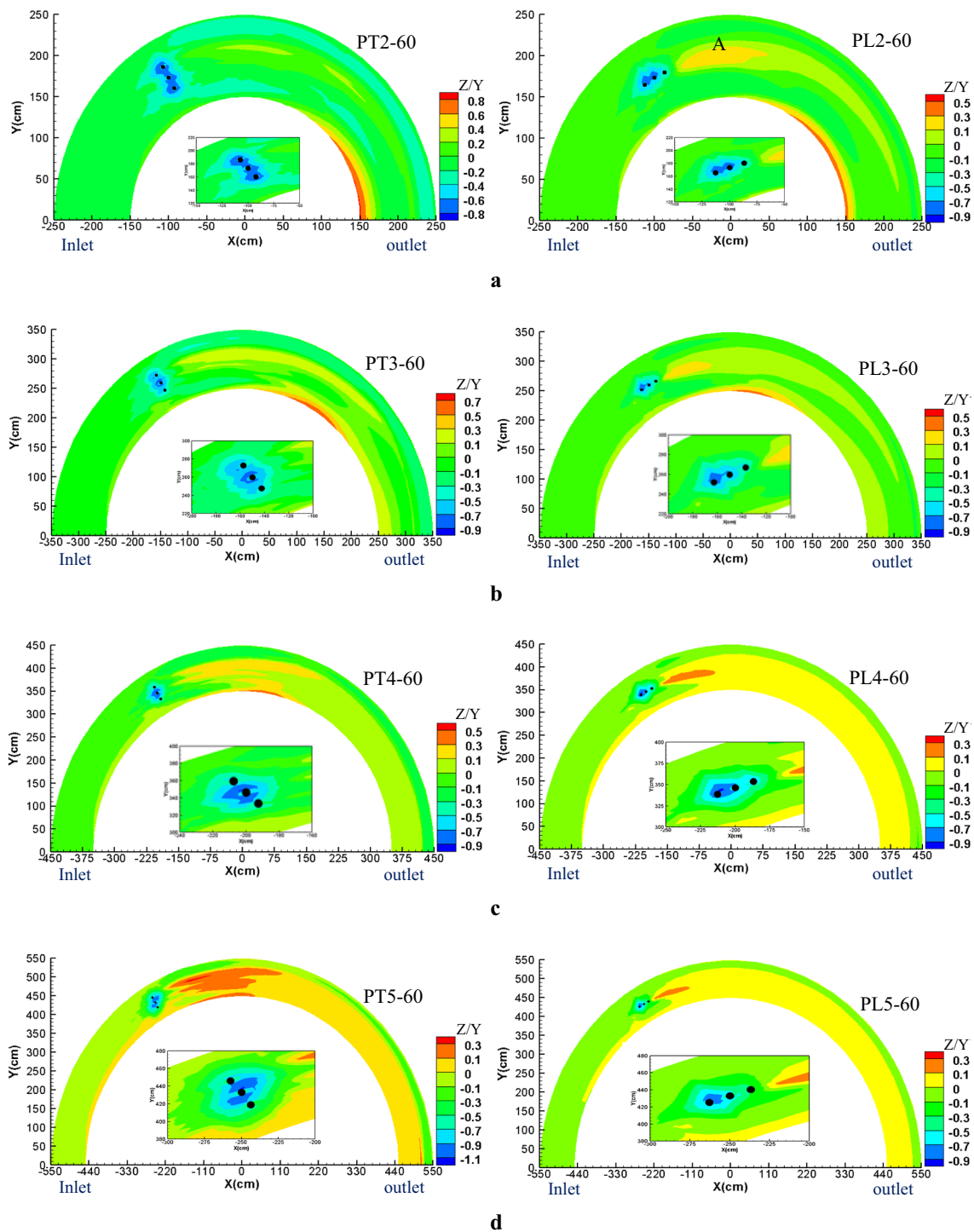


Fig. 6 Bed topography when the piers are placed at the 60-degree position and the relative radius is **a** 2, **b** 3, **c** 4 and **d** 5

with respect to the flow direction from transverse to longitudinal, the maximum depth of scour hole deteriorated about 13%. In PT2-60, the sedimentary stacks and the location of the maximum height of sedimentation are highlighted near the inner bank; however, in PL2-60, another main sedimentary stack is developed near the outer bank at the pier

downstream in area “A.” This is due to sediment removal from the scour hole. The pier arrangement results in the flow redirection and is consequently responsible for the formation of the unsymmetrical scour hole. As presented in Fig. 6b, the pier positional change from transverse to longitudinal direction to the flow in the sharp bend with $R = 3B$ makes the

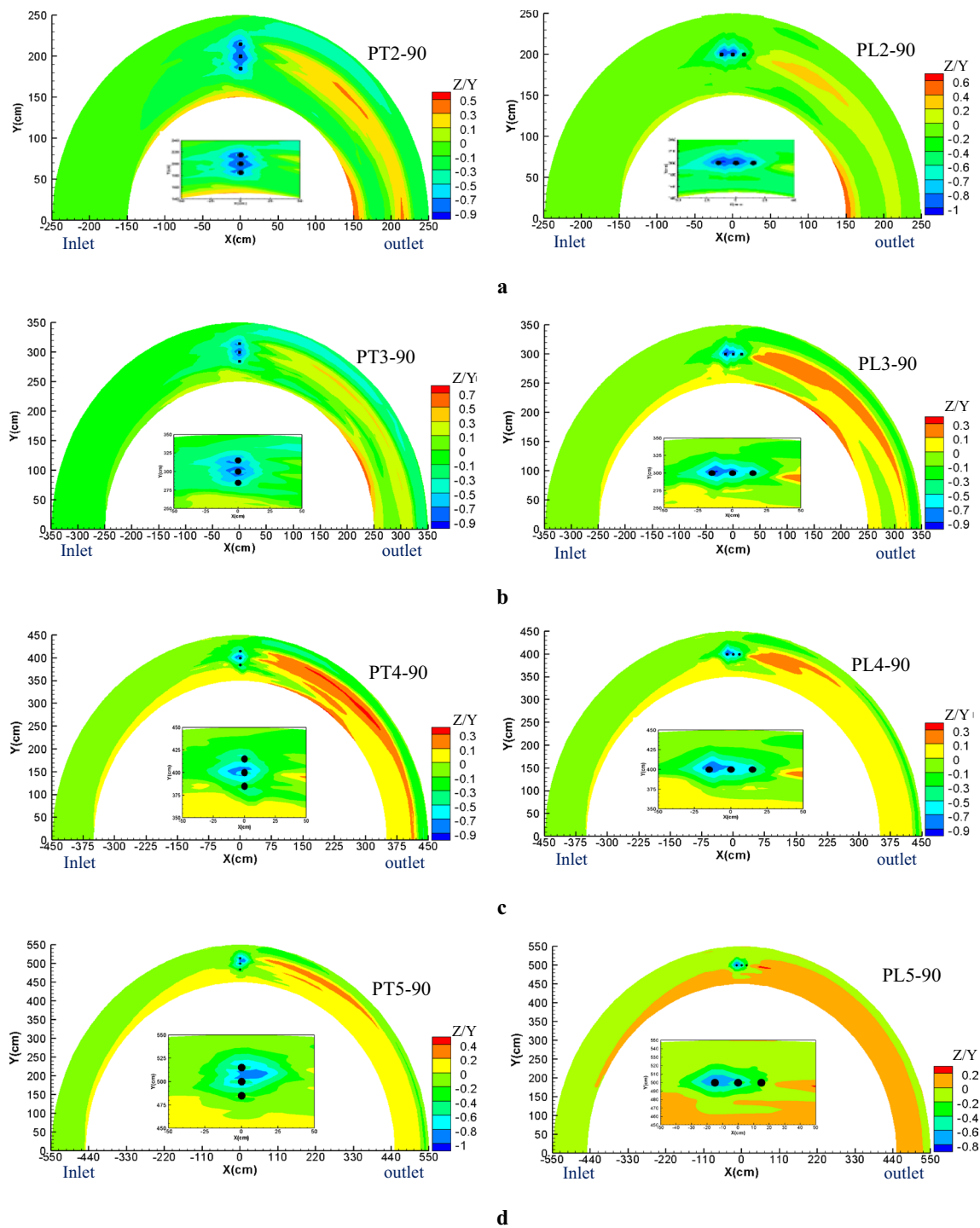


Fig. 7 Bed topography when the piers are placed at the 90-degree position and the relative radius is **a** 2, **b** 3, **c** 4 and **d** 5

maximum scour and sedimentation reduced by 2 and 45%, respectively, whereas increasing the relative radius to 4, based on Fig. 6c, causes 0 and 44% growth in the maximum scour and sedimentation, respectively. In effect, the piers in transverse position induce remarkable bed variations in comparison with those in a longitudinal arrangement. Where

$R = 5B$, as given in Fig. 6d, and if the arrangement of piers located at the 60-degree section is changed from transverse to longitudinal with respect to the flow direction, the maximum scour is declined by 24%, while the scour hole around the piers through the flume width in PL5-60 is extended further than that in PT5-60.

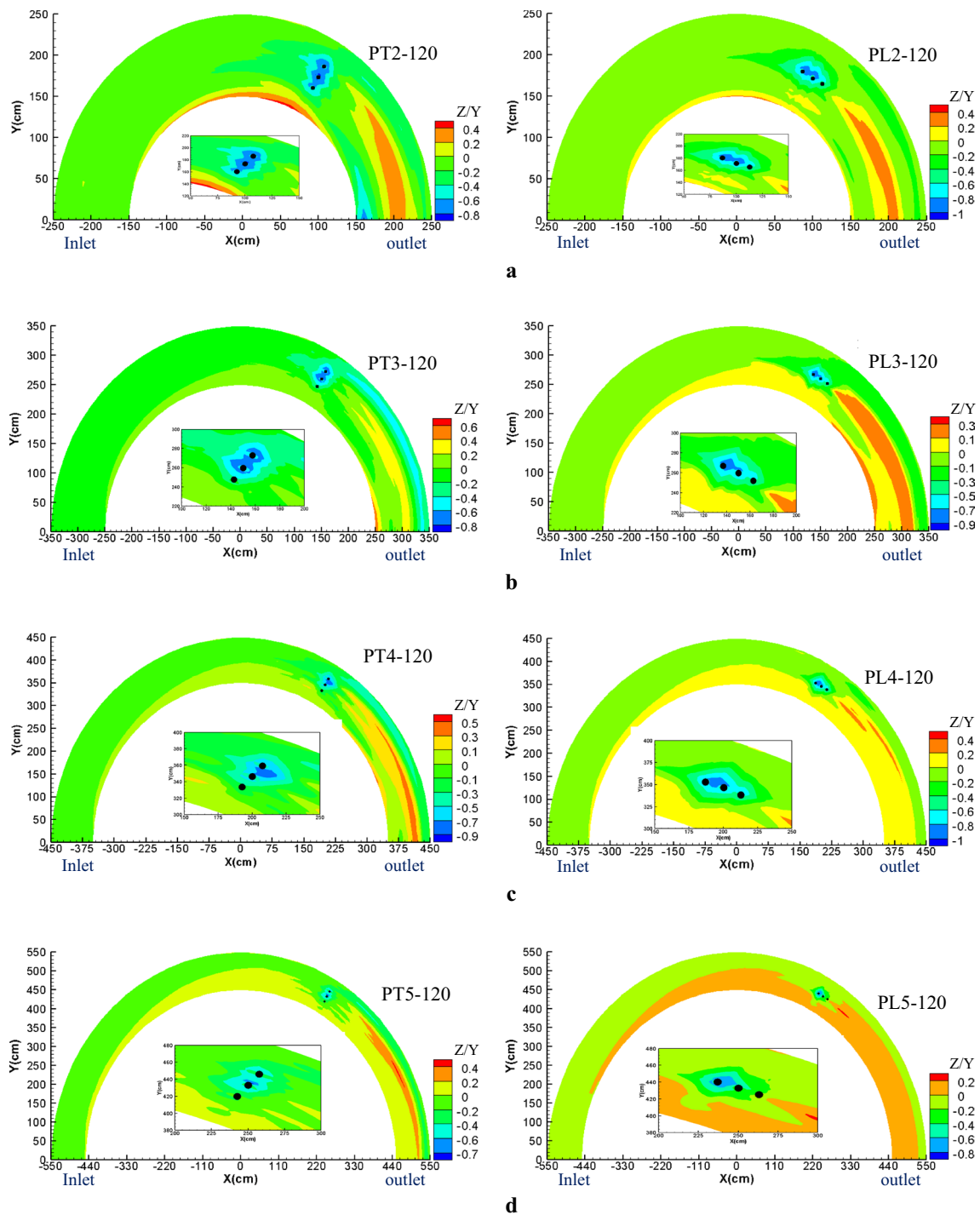


Fig. 8 Bed topography when the piers are placed at the 120-degree position and the relative radius is a **2**, **b** 3, **c** 4 and **d** 5

According to Fig. 7a, when the piers are placed in the bend apex in transverse direction to flow, the maximum scour depth around the piers in comparison with the longitudinal ones is estimated to rise and obviously extends the sediment accumulated along the downstream inner bank. Similarly, adjacent to the outer bank at the piers downstream

in PT2-90, a secondary scour hole with the maximum scour depth of $0.45Y$ is reported. Here, more erosion in response to the flow stream deflected toward the outer bank is indicated. The sedimentary stacks resulting from bed excavation around the bridge pier at the inner bank and in the middle of the flume are displayed in Fig. 7b. The maximum scour

improvement is associated with a change in the relative radius around the piers placed in transverse direction to the flow; however, in the case with piers located in a longitudinal direction to the flow, it is totally different, for the relative radius increases from 2 to 3 and the maximum height of sedimentary stack decreases by 42%. In Fig. 7c, for PT4-90, the maximum scour depth along the flume takes place around the pier located at a shorter distance away from the outer bank at $\theta = 89^\circ$ position although for PL4-90, it happens around the middle pier at $\theta = 88^\circ$ position. This phenomenon could be affected by the pier position with respect to the direction of the maximum flow velocity. According to Fig. 7d, some factors such as the turbulent cross-flow, downward flow and formation of vortices around the piers are involved in the maximum scour. This amount in PT5-90 and PL5-90 is, respectively, $0.96Y$ and $0.8Y$, and an adjustment in the pier installation from transverse to longitudinal makes the scour 2.5° closer to the bend entrance. In addition, development of the scour hole around the downstream bridge pier in PT5-90 compared to PL5-90 increases by 30%.

When the bridge piers are installed at the 120° position and $R = 2B$, as given in Fig. 8a, the scour depth is directly proportional to the size of the scour hole. The maximum scour hole extension has been recorded in PL2-120 that has been extended $6.5D$ from the pier position toward downstream. In Fig. 8b, although the maximum scour depth around the piers in PL4-120 is greater than that in PT4-120, in the latter, the scour hole around downstream piers is extended 0.16 times further than that in the former. This

could be associated with more downward currents in PT4-120; however, because of the pier arrangement in PL4-120, the bed is exposed to more downward flow. Hence, it creates a deeper hole in front of the piers and, eventually, PL4-120 experiences fewer fluctuations in bed at the downstream piers compared to PT4-120. In Fig. 8c, regarding the bed elevation, a 15% increase in the maximum scour depth and a change in the pier direction from transverse to longitudinal to the flow in two certain models lead to a 34% reduction in sedimentation level, which is due to the effect of the bend and the piers on the flow pattern. This trend has also been recorded in Fig. 8d, with piers in the mild bend ($R = 5B$), so that changing the pier direction from transverse to longitudinal causes 14% growth in the maximum scour depth as well as 45% reduction in the maximum sedimentation level. The point worth noting is that the pier arrangement in PL5-120 results in lower intensity of the secondary flow downstream to prevent the formation of the secondary scour hole.

3.2 The Maximum Scour Depth and the Occurrence Location

Figure 9 displays the maximum scour position in the bend for all models. As obvious, the maximum scour variations range from $0.7Y$ to $1.14Y$, which occur in PT5-120 and PT5-60 at 120° and 60° , respectively, where the piers are installed. Besides, the maximum scour depths are smaller in piers placed in transverse direction to the flow compared to piers in longitudinal direction to the flow.

Fig. 9 Position and the maximum scour depth around the bridge piers, non-dimensionalized with respect to the flow depth at bend entrance

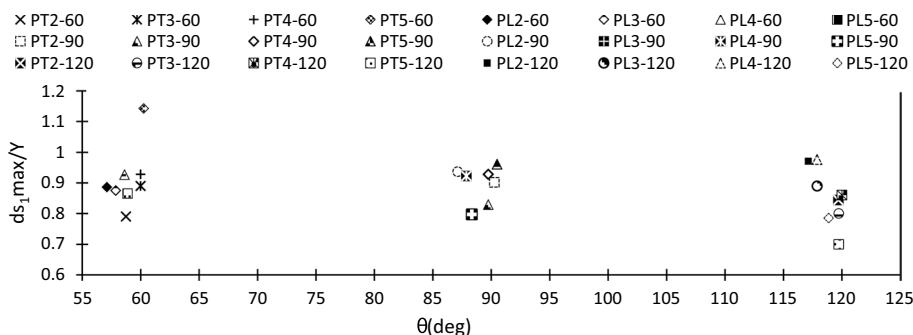
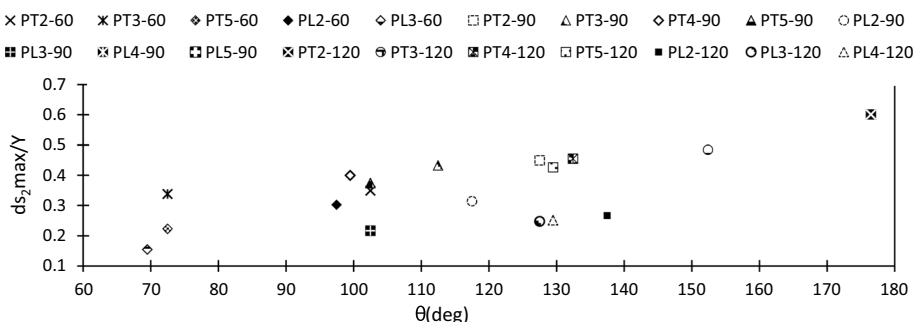


Fig. 10 Location of the maximum secondary scour hole depth around the bridge piers, non-dimensionalized with respect to the flow depth at the bend entrance



3.3 Depth of the Secondary Scour Hole and Its Position

In Fig. 10, the maximum scour depth of the existing secondary hole at the downstream piers has been marked. As presented, the maximum scour depth of the second hole occurs at $\theta = 69.5^\circ - 150^\circ$ at a distance of 31–75% of the flume width from the inner bank. The maximum depth of the secondary scour hole is recorded only in PT2-120, at $\theta = 176.5^\circ$ and at a distance of 10% of the flume width from the outer bank. The reason behind this is that the piers approaching the sharp bend exit with $R = 2B$ generate the velocity distribution, and the maximum velocity is deflected toward the outer bank owing to the presence of the downstream reach of path. The maximum and minimum depths of the second scour hole for PT2-120 and PL3-60 are $0.6Y$ and $0.15Y$, respectively. In other words, considering Fig. 10, in PT4-60, PL4-60, PL5-60 and PL5-120, there is no scour hole generated at the downstream side of the piers.

3.4 The Maximum Height of Sedimentation and Its Position

The maximum height of sedimentary stacks is provided in Fig. 11. In all simulated models, with piers placed in transverse direction to the flow, except for PT2-120, the maximum height of sedimentation compared to the cases with piers placed in a longitudinal direction to the flow forms farther away with respect to the pier position. For instance, for piers located at $\theta = 90^\circ$ with $R = 4B$, for cases with piers placed in both transverse and longitudinal directions to flow, the maximum height of sedimentary stacks is detected at distances of $26D$ and $47D$ from the pier location. With regard to the maximum height of sedimentation for all models except PT2-90, this point in models with piers located in transverse direction to flow is higher than that in cases with piers placed in a longitudinal direction to the flow.

Fig. 11 Location and the maximum relative height of sedimentation, non-dimensionalized with respect to the flow depth at the beginning of the bend

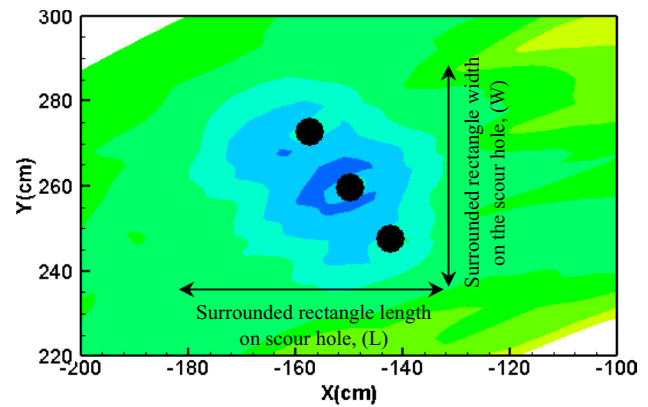
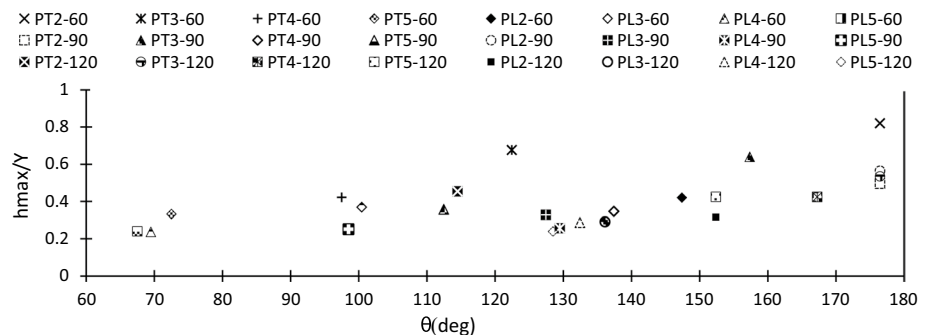


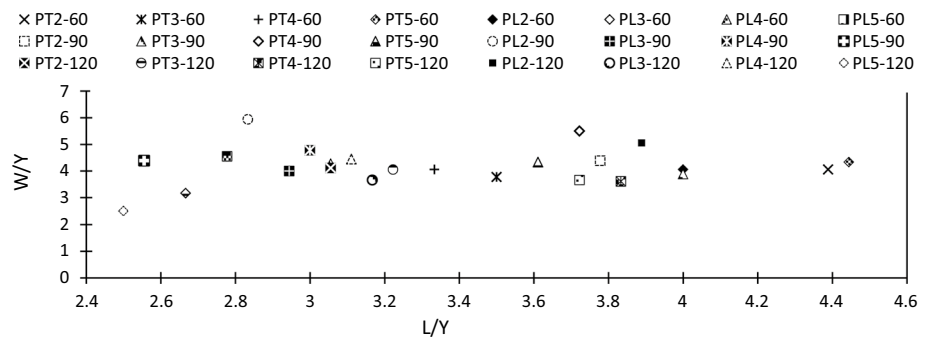
Fig. 12 A schematic view of the rectangle surrounding the scour hole around the piers

3.5 Dimensions of the Rectangle Surrounding the Scour Hole

In order to study the impact of the relative radius and the pier position in both piers in transverse and longitudinal directions to the flow on the scour hole distribution in both width and length of flume, the surrounding rectangle dimensions are given in Fig. 12. For the estimation of the scour hole location, points in which the scour depth is greater than 50% of the pier diameter (deeper than 2.5 cm) are assumed to be associated with the main scour hole around the piers. A schematic view of the surrounding rectangle is shown in Fig. 12.

Figure 13 displays the schematic view of the rectangle surrounding the scour hole around the bridge piers. The horizontal and vertical axes present the dimensionless length and width of the rectangle, respectively. As shown in the figure, the length and width of this rectangle are equal in PL5-120 so that a square-shaped scour hole is produced around the pier. In PT2-60, the length of the rectangle is greater than its width. As such, the longitudinal sediment accumulation is more visible than the lateral one. For all models, the length of the surrounding rectangle ranges from 2.5 to 4.5 times the flow depth, which peaks in PT5-60 and reaches the

Fig. 13 Dimensions of the rectangle surrounding the scour hole around the piers

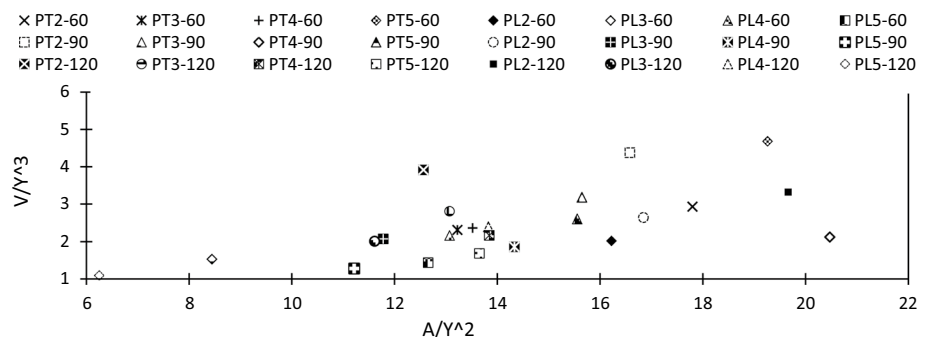


minimum in PL5-120. Width of the surrounding rectangle peaks in PL2-90 and reaches the minimum in PL5-120.

3.6 Scour Hole Area and Volume

To display the scour hole size around the piers, the figure related to the area and the volume of the scour hole around the piers, non-dimensionalized with the second and third powers of the flow depth at the bend entrance in all models, is displayed in Fig. 14. Considering Fig. 14, the maximum dimensionless area of the scour hole around the piers is detected in PT4-90. It is argued that in the case with pier groups placed in a transverse direction to the flow, in a mild bend with a relative radius of $R=4B$, the more the piers approach the bend apex, the more expanded the scour hole appears so that the area of scour hole around piers in PT4-90 has been reported 34 and 32% greater than those in PT4-60 and PT4-120, respectively. A comparison between the maximum scour depth and hole development indicates that, in some cases, these two variables variations are totally different. For example, although the maximum scour depth around piers in PL3-90 is about 10% greater than that of PT3-90 (Fig. 9), regarding Fig. 14, the scour hole is 32% less expanded in PL3-90 compared to PT3-90. Also, the maximum volume non-dimensionalized with respect to the cube of the flow depth belongs to PT5-60, whereas the minimum one is recorded in PL5-120, and they are 5 and 1, respectively.

Fig. 14 Dimensionless scour surface area and the scour hole volume around the piers



3.7 Longitudinal Sections of Scour

Figure 15 depicts the drawn sections at a distance of 5% of the channel width from the inner bank along the bends with different relative radii with piers placed in different locations. In the sharp bend given in Fig. 15a, the maximum scour has occurred at the end of the channel. In this section, the maximum scour is estimated $0.5Y$ and belongs to PT2-120 at $\theta=175.5^\circ$ position of the bend. In these sections, the sedimentation is observed from the 25-degree angle to the end of the bend. This phenomenon is more evident in the second half of the bend and downstream of piers. This is due to the fact that the excavated materials from the scour hole coincide with the maximum velocity in the bend and deflects the sediments toward the inner bank. The maximum height of sedimentary stacks in these sections is $0.55Y$ at $\theta=122^\circ$ position in PT3-60, and the pier relocation to 90° , with the same arrangement (PT3-90), results in height reduction by 9%, as shown in Fig. 15b. As depicted in Fig. 15c, in all models from 0° to 60° from the beginning of bend, the bed variations follow the same trend. The maximum height of the sedimentary stack is $0.3Y$ and belongs to PT4-60 at $\theta=97.5^\circ$ position. In the mentioned model, from the 120-degree angle until the bend end, the bed elevation remains unchanged. As shown in Fig. 15d, patterns of the bed elevation variations in models with piers placed in a transverse direction to the flow are similar and the variations start at shorter distance to the beginning of the bend compared to those in the models with piers placed in a longitudinal direction to the flow.

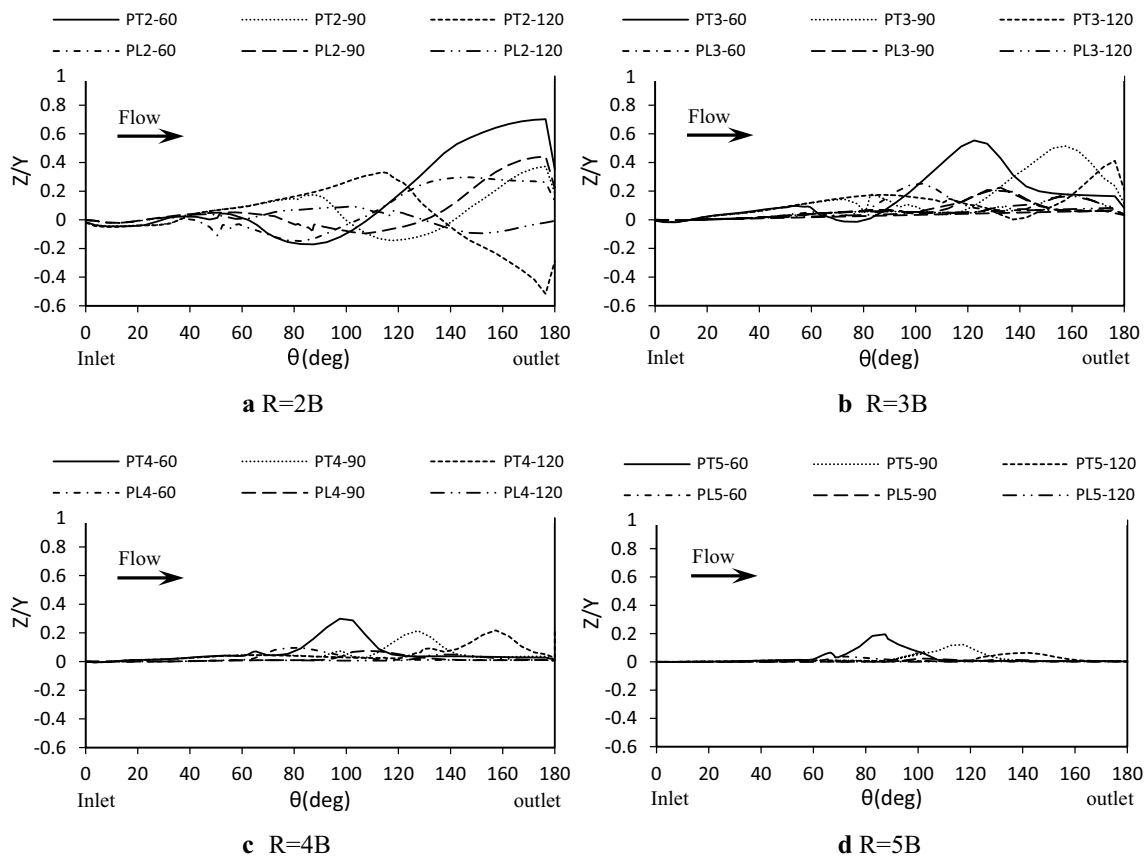


Fig. 15 A sample of longitudinal sections at a distance of 5% of the flume width from the inner bank in models with curve radii of **a** 2, **b** 3, **c** 4 and **d** 5

Moreover, unlike the sharp bend, the scour does not occur near the inner bank when $R = 5B$.

In the cross section crossing the middle of the channel, regarding Fig. 16a, the main scour hole and its development along the flume are obtained. By changing the pier arrangement from transverse to longitudinal, a remarkable reduction in the depth of the scour hole is visible. A little farther away from the piers, at the piers downstream, the sediments start to deposit. The maximum height of sediment, $0.3Y$, occurs in the middle of the flume, for PT3-120 and at $\theta = 152^\circ$, as shown in Fig. 16b. By moving the piers placed in transverse direction to the flow from the first half of the bend to the second half, based on Fig. 16c, there is less scour in the middle of the flume and around the piers; however, the model with the piers situated in a longitudinal direction to the flow yields an inverse response so that the scour hole depth in PL4-120 is about 5% greater than that in PL4-60. When $R = 5B$, according to Fig. 16d, in both pier arrangements, the scour hole depth decreases from the first half to the second half of bend.

Figure 17 illustrates the longitudinal sections near the outer bank for all models. In all cases, the scour happens in the second part of the bend, near the outer bank. In fact,

the scour occurs periodically. Regarding the flow deflection toward the outer bank, the scour hole formation near the outer bank is explainable. The minimum scour depth is reported to be $0.1Y$ in PL2-60 and PL3-60 and the maximum, due to a change in the pier situation, is $0.4Y$ in PT3-120, as shown in Fig. 17a, b. By changing the relative curvature radius of the bend from 2 and 3 to 4 and 5, as in Fig. 17c, d, the holes formed in the mild bend are steeper compared to those in the sharp bend. The hole slope toward the inner and outer banks follows falling and rising trends, and the bed topography variations in the mild bend are less than those in a sharp bend. The maximum depth of scour hole in the outer bank is $0.38Y$ and is attributed to PT4-120 at $\theta = 130^\circ$.

4 Discussion

By comparing Figs. 6, 7 and 8, it can be stated that when the flow hits the bridge pier nose, the flow velocity changes into pressure on pier. Due to distribution of transverse flow velocity and upward increasing velocity, a downward high-pressure gradient is induced at the pier. The maximum

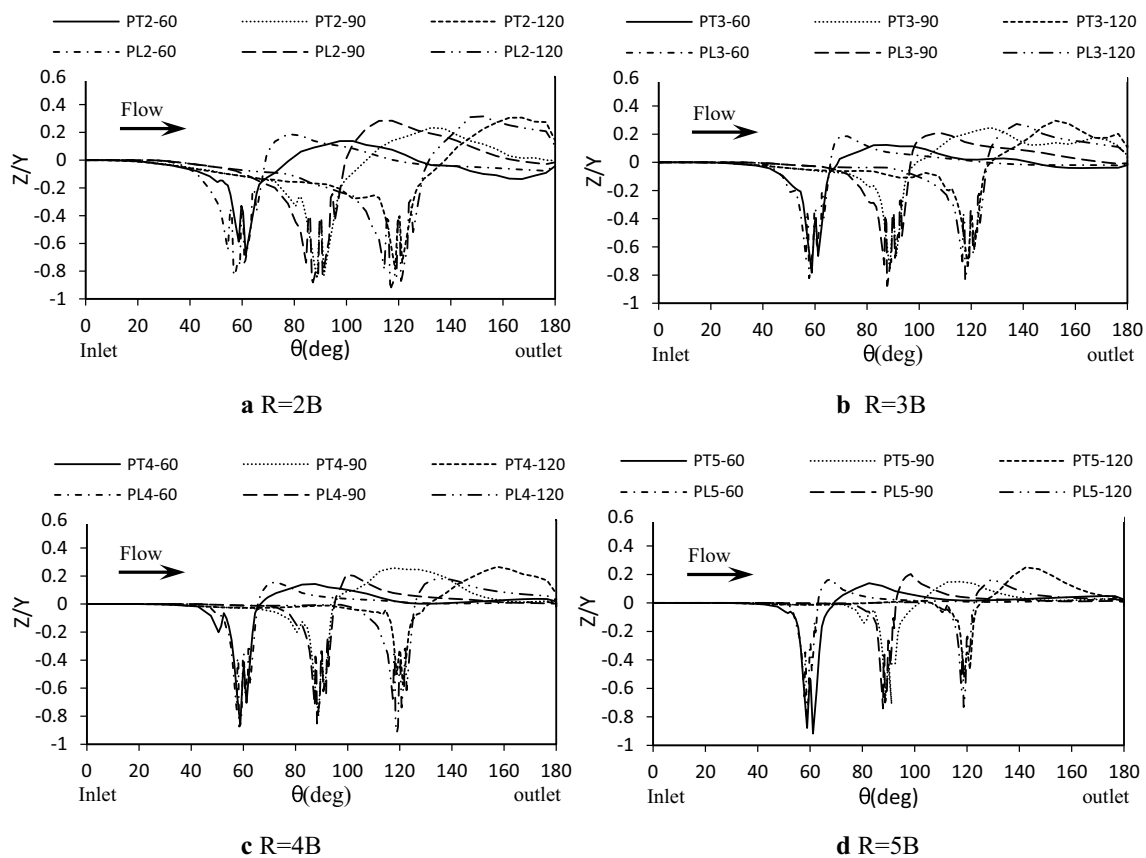


Fig. 16 A sample of longitudinal sections at a distance of 50% of the flume width from the inner bank in models with curvature radii of **a** 2, **b** 3, **c** 4 and **d** 5

scour, in all relative curvature radii, happens around the piers because the pressure gradient produces a down-flow at the front of the pier. Also, the presence of piers placed in a transverse direction to the flow at the beginning of the channel can affect bed topography variations more than those in a longitudinal direction. This is due to the presence of more obstacles on the flow in the former case compared to the latter. Consequently, significant variations are created in the bed topography. As for sedimentation, regarding the flow characteristics of the bend and the presence of close-bed flows moving toward the inner bank, the area is one where the maximum sedimentation would occur. Furthermore, according to observations, relocating the piers from the first half of bend to the second half would lead to the formation of abutments at a shorter distance from the piers.

Comparing the outcomes of the numerical analysis related to the position, the maximum scour depth value and the maximum sedimentation height in Figs. 9 and 11, it can be stated that an average increase in the maximum scour value and sedimentation around the piers installed in both transverse and longitudinal directions to the flow is associated with increasing the relative curvature radius from 2 to 5. Relocating the piers from the first half of bend to the apex

of the bend (from 60° to 90°) and to the second half of bend (120°) leads to an increase in the maximum scour.

For all the models depicted in Fig. 10, a comparison of the secondary scour hole among the models illustrates that the second scour hole in addition to the main scour hole is formed at the outer bank at the downstream face of the piers. However, for piers placed in a longitudinal direction to the flow, the second scour hole occurs at the upstream side of the piers at outer bank only in PL2-90, PL2-60, PL2-120, PL3-120 and PL4-120. The largest second scour hole forms in PT2-120, at the 176.5-degree position at the distance of 0–10% of the channel width from the inner bank, whereas the smallest one is seen in PT5-60, at 102.5°. In general, increasing the relative curvature radius and using a milder 180-degree bend entail a shallower second scour hole which occurs at a short distance to the pier.

In Fig. 13, the width of the rectangle surrounding the scour hole formed around the piers is longer than its length in the models in which the piers are placed in a transverse arrangement. As such, with this pier arrangement, the latitudinal flow is stronger, and accordingly, the sediments move toward the latitudinal axis of the channel rather than the longitudinal axis. The maximum length of

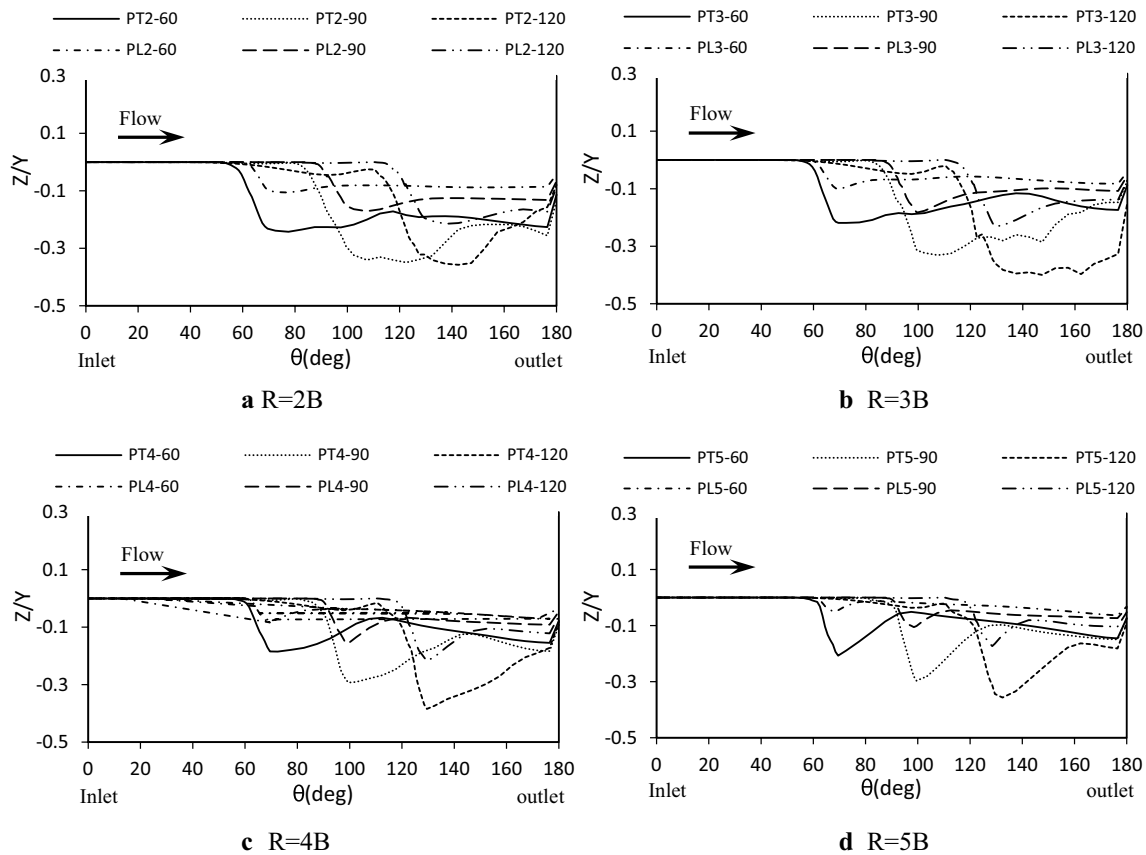


Fig. 17 A sample of longitudinal sections at a distance of 95% of the flume width from the inner bank in models with curvature radii of **a** 2, **b** 3, **c** 4 and **d** 5

the rectangle surrounding the scour hole is in PT5-60 and the minimum is obtained in PL5-120, the values of which equal 4.5 and 2.5 times the flow depth at the beginning of the bend, respectively. Moreover, observations indicate that the length and width of the rectangle in the model with piers placed in a longitudinal direction to the flow at the 120-degree position from the beginning of the bend with a relative curvature radius of 5 have been equal. In other words, the scour hole is surrounded by a square. It could be argued that in order for the flow strength to transfer sediments around bridge piers, length and width of channel are the same.

Investigation of the area and the volume of the scour hole displayed in Fig. 14 demonstrates that the area and the dimension of the scour hole around the piers placed in a transverse direction to the flow are greater than those with the piers in a longitudinal direction to the flow (except in the model with piers placed at 120° in a sharp bend). Actually, in the case with piers located in a transverse direction to the flow, owing to the frequent collision of the flow to piers and the resultant turbulent flow, the wider scour hole is produced along both channel length and width. Moreover, the variations appear in the scour hole volume around piers

as a stronger down-flow is generated around the piers placed in a transverse direction to the flow.

Considering profiles crossing at distances of 5, 50 and 95% of the channel width from the inner bank in Figs. 15, 16 and 17, it is evident that the bed topography variations in the case with piers placed in a transverse direction to the flow are more considerable than the ones in a longitudinal direction to the flow, and using a milder bend results in less sedimentation at the inner bank. In the middle of the channel, the scouring is more visible than in other profiles because of the presence of vortices around bridge piers. Similarly, from the beginning of the channel to the 50-degree position from the bend entrance, there are no notable changes near the outer bank in all the models. Subsequently, due to the flow attack toward the outer bank, the scour holes are consecutively developed until the end of the bend.

5 Conclusion

The main purpose of this manuscript is to examine scouring around cylindrical piers placed in both transverse and longitudinal directions to the flow in a 180° bend, and validation

has been performed using experimental data. Some effective parameters such as the position and direction of the piers and the relative radius have been measured. The results are listed below:

Results of verification show that SSIIM numerical model efficiently estimates the value and position of the maximum scour and the maximum sedimentation when piers are placed in a longitudinal direction to the flow using a similar experimental model. It proves that SSIIM is capable of simulating bed topography in a bend with pier groups inside.

Generally, in a sharp 180-degree bend with piers placed in a longitudinal direction to the flow, the maximum scour value is recorded greater than those with piers located in a transverse direction to the flow, regardless of the relocation of the piers. This phenomenon is also observed in a bend with a relative radius of 3, except when the piers are placed at the 60-degree position. However, for the other relative radii, there have been notable feature recorded in the maximum scour depth variations, which is associated with the pier arrangement.

The maximum scour depth around the piers for models with piers located in transverse and longitudinal directions to the flow in PT5-60 and PL4-120 has been equal to 1.14 and 0.98 times the flow depth at the first half of the bend, respectively, measured at 60- and 119-degree positions from the bend entrance.

For all the models with piers placed in a transverse direction to the flow, the pier located at a shorter distance from the outer bank is subject to the maximum scour; however, in the models with piers oriented in a longitudinal direction to the flow, this phenomenon occurred around the middle pier.

On the whole, the maximum height of sedimentary stacks for the model in which the piers are placed in a transverse direction to the flow is greater compared to those in a longitudinal arrangement, except in PT2-90. Also, the maximum and minimum heights of sedimentary stacks have been determined in PL2-60 and PL4-60, which were equivalent to 0.8 and 0.2 times the flow depth at the bend entrance, and were observed at 176 and 69° positions of the bend, respectively.

The maximum length of the rectangle surrounding the scour hole was measured in PT2-60, which was equal to 4.5 times the flow depth at the beginning of the bend. Moreover, for PL5-120, the length and width of the rectangle were 2.5 times the flow depth at the beginning of the bend, while the square-shaped scour hole appeared.

Relocating piers from transverse to longitudinal directions to flow led to a reduction in the expansion and the volume of scour hole developed around piers so that the maximum area of scour hole around the piers occurring in PT4-90 model was equal to 20.5 times the square of the flow depth at the beginning of the bend. Additionally, the minimum and maximum scour hole volumes around the bridge

pier were reported 1 and 5 times the cube of the incoming flow depth, respectively, for PL5-120 and PT5-60 models.

References

- Akib S, Basser H, Karami H, Jahangirzadeh A (2014) Retrofitting of bridge piers against the scour damages: case study of the Marand-Sooofian route bridge World Academy of Science, engineering and technology. *Int J Civ Archit Sci Eng* 8:56–60. <https://doi.org/10.5281/zenodo.1336432>
- Asadollahi M, Vaghefi M, Tabib nejad Motlagh MJ (2019) Experimental and numerical comparison of flow and scour patterns around a single and triple bridge piers located at a sharp 180 degrees Bend. *Scientia Iranica*. <https://doi.org/10.24200/SCI.2019.5637.1391>
- Asadollahi M, Vaghefi M, Akbari M (2020) Effect of the position of perpendicular pier groups in a sharp bend on flow and scour patterns: numerical simulation. *J Braz Soc Mech Sci Eng* 42(8):1–15. <https://doi.org/10.1007/s40430-020-02503-2>
- Azizi S, Farsadzadeh D, Arvanaghi H, Abbaspour A (2016) Numerical simulation of flow pattern around the bridge pier with submerged vanes. *J Hyd Struct* 2(2):46–61. <https://doi.org/10.22055/JHS.2016.12856>
- Basser H, Cheraghi R, Karami H, Ardeshir A, Amir mohajedi M, Akib S, Shamshirband S, (2015) Modeling sediment transport around a rectangular bridge abutment. *Environ Fluid Mech* 15(6):1105–1114. <https://doi.org/10.1007/s10652-015-9398-z>
- Ben Mohammad Khajeh Sh, Vaghefi M (2020) Investigation of abutment effect on scouring around inclined pier at a bend. *J Appl Water Eng Res*. <https://doi.org/10.1080/23249676.2020.1761898>
- Ben Mohammad Khajeh Sh, Vaghefi M, Mahmoudi A (2017) The scour pattern around an inclined cylindrical pier in a sharp 180-degree bend: an experimental study. *Int J River Basin Manag* 15(2):207–218. <https://doi.org/10.1080/15715124.2016.1274322>
- Bozkus Z, Yildiz O (2004) Effects of inclination of bridge piers on scouring depth. *J Hyd Eng* 130(8):822–827
- Ehteram M, Meymand AM (2015) Numerical modeling of scour depth at side piers of the bridge. *J Comput Appl Math* 280:68–79. <https://doi.org/10.1016/j.cam.2014.11.039>
- Elsaeed GH (2011) Validating SSIIM 3-D numerical model to calculate local scour around bridge piers. *Int J Acad Res* 3(3):501–505
- Elsebaie IH (2013) An experimental study of local scour around circular bridge pier in sand soil. *Int J Civ Environ Eng* 13(1):23–28
- Ezzeldin RM (2019) Numerical and experimental investigation for the effect of permeability of spur dikes on local scour. *J Hydro inform* 21(2):335–342. <https://doi.org/10.2166/hydro.2019.114>
- Fael C, Lança R, Cardoso A (2016) Effect of pier shape and pier alignment on the equilibrium scour depth at single piers. *Int J Sedim Res* 31(3):244–250. <https://doi.org/10.1016/j.ijsrc.2016.04.001>
- Ghobadian R, Basiri M (2016) The effect of downstream curved edge on local scouring at 60-degree open channel junction using SSIIM1 model. *Ain Shams Eng J* 7(2):543–552. <https://doi.org/10.1016/j.asej.2015.06.001>
- Graf WH, Istiarto I (2002) Flow pattern in the scour hole around a cylinder. *J Hydraul Res* 40(1):13–20. <https://doi.org/10.1080/00221680209499869>
- Hamidi A, Siadatmousavi SM (2017) Numerical simulation of scour and flow field for different arrangements of two piers using SSIIM model. *Ain Shams Eng J* 9(4):2415–2426. <https://doi.org/10.1016/j.asej.2017.03.012>
- Hämmerling M, Walczak N, Nowak A, Mazur R, Chmist J (2018) Modelling velocity distributions and river bed changes using computer code SSIIM below sills stabilizing the riverbed. *Pol J Environ Stud* 28(3):1165–1179. <https://doi.org/10.15244/pjoes/85224>

- Johnson PA, Dock DA (1998) Probabilistic bridge scour estimates. *J Hyd Eng* 124(7):750–754. [https://doi.org/10.1061/\(ASCE\)0733-9429\(1998\)124:7\(750\)](https://doi.org/10.1061/(ASCE)0733-9429(1998)124:7(750))
- Karimi N, Heidarnejad M, Masjedi A (2017) Scour depth at inclined bridge piers along a straight path: a laboratory study. *Eng Sci Technol Int J* 20(4):1302–1307. <https://doi.org/10.1016/j.jestch.2017.07.004>
- Khayyun TS, Mouhamed NH (2018) Three dimensional modeling of sediment transport upstream of Al- Betera regulator-Iraq. *J Eng Sustain Dev* 22(5):215–238. <https://doi.org/10.31272/jeasd.2018.5.16>
- Leschziner MA, Rodi W (1979) Calculation of strongly curved open channel flow. *J Hyd Div* 105(10):1297–1314
- Mohamed YA, Nasr Allah TH, Abdel Aal GM, Awad AS (2015) Investigating the effect of curved shape of bridge abutment provided with collar on local scour, experimentally and numerically. *Ain Shams Eng J* 6(2):403–411. <https://doi.org/10.1016/j.asej.2014.10.011>
- Olsen NRB (2014) A three-dimensional numerical model for simulation of sediment movement in water intakes with multi-block option. Department of Hydraulic and Environmental Engineering, Norwegian University of Science and Technology, User's manual, Norway, pp172–183
- Olsen NRB, Melaaen MC (1993) Three-dimensional calculation of scour around cylinders. *J Hyd Eng* 119(9):1048–1054. [https://doi.org/10.1061/\(ASCE\)0733-9429\(1993\)119:9\(1048\)](https://doi.org/10.1061/(ASCE)0733-9429(1993)119:9(1048))
- Rasaei M, Nazari S, Eslamian S (2020) Experimental and numerical investigation the effect of pier position on local scouring around bridge pier at a 90° convergent bend. *J Hyd Struct* 6(1):55–76. <https://doi.org/10.22055/JHS.2020.32753.1134>
- Richardson JE, Panchang VG (1998) Three-dimensional simulation of scour-inducing flow at bridge piers. *J Hyd Eng* 124(5):530–540. [https://doi.org/10.1061/\(ASCE\)0733-9429\(1998\)124:5\(530\)](https://doi.org/10.1061/(ASCE)0733-9429(1998)124:5(530))
- Roulund A, Sumer BM, Fredsoe J, Michelsen J (2002) 3-D numerical modeling of flow and scour around a pile. In: First international conference on scour of foundations international society of soil mech and foundations
- Salahedin TM, Imran J, Chaudhry MH (2004) Numerical modeling of three-dimensional flow field around circular piers. *J Hyd Eng* 130(2):91–100. [https://doi.org/10.1061/\(ASCE\)0733-9429\(2004\)130:2\(91\)](https://doi.org/10.1061/(ASCE)0733-9429(2004)130:2(91))
- Tseng MH, Yen CL, Song CC (2000) Computation of three-dimensional flow around square and circular piers. *Int J Numer Meth Fluids* 34(3):207–227. [https://doi.org/10.1002/1097-0363\(20001015\)34:3%3c207::AID-FLD31%3e3.0.CO;2-R](https://doi.org/10.1002/1097-0363(20001015)34:3%3c207::AID-FLD31%3e3.0.CO;2-R)
- Vaghefi M, Safarpour Y, Akbari M (2017) Numerical comparison of the parameters influencing the turbulent flow using a T-shaped spur dike in a 90° bend. *J Appl Fluid Mech* 10(1):231–241. <https://doi.org/10.18869/acadpub.jafm.73.238.26175>
- Vaghefi M, Tabib Nazhad Motlagh MJ, Sh HS, Moradi S (2018) Experimental study of bed topography variations due to placement of a triad series of vertical piers at different positions in a 180° bend. *Arab J Geosci* 11(5):102. <https://doi.org/10.24200/SCI.2019.5637.1391>
- Vaghefi M, Solati S, Abdi Chooplou Ch (2020) The effect of upstream T-shaped spur dike on reducing the amount of scouring around downstream bridge pier located at a 180° sharp bend. *Int J River Basin Manag*. <https://doi.org/10.1080/15715124.2020.1776306>
- Wang H, Tang H, Liu Q, Wang Y (2016) Local scouring around twin bridge piers in open-channel flows. *J Hyd Eng* 142(9):06016008. [https://doi.org/10.1061/\(ASCE\)HY.1943-7900.0001154](https://doi.org/10.1061/(ASCE)HY.1943-7900.0001154)
- Yen CL, Lai JS, Chang WY (2001) Modeling of 3D flow and scouring around circular piers. *Proc Natl Sci Council Roc (A)* 25(1):17–26